Inorganic Chemistry

Article

pubs.acs.org/IC

Hydroxido-Supported and Carboxylato Bridge-Driven Aggregation for Discrete $[Ni_4]$ and Interconnected $[Ni_2]_n$ Complexes

Krishna Chattopadhyay,[†] Gavin A. Craig,[‡] Animesh Kundu,[†] Valerio Bertolasi,[§] Mark Murrie,[‡] and Debashis Ray*[,†]

[†]Department of Chemistry, Indian Institute of Technology, Kharagpur 721 302, India

[‡]School of Chemistry, University of Glasgow, Glasgow G12 8QQ, United Kingdom

[§]Dipartimento di Scienze Chimiche e Farmaceutiche, Centro di Strutturistica Diffrattometrica, University of Ferrara, 44121 Ferrara, Italy

Supporting Information

ABSTRACT: Four different carboxylato bridges have been efficiently utilized for growth of three tetranuclear nickel(II) complexes $[Ni_4(\mu_3\text{-}H_2L)_2(\mu_3\text{-}OH)_2(\mu_{1,3}\text{-}CH_3CO_2)_2](ClO_4)_2$ (**1**), $[Ni_4(\mu_3\text{-}H_2L)_2(\mu_3\text{-}OH)_2(\mu_{1,3}\text{-}C_2H_5CO_2)_2](ClO_4)_2\cdot 1/2H_2O$ (**2**), and $[Ni_4(\mu_3\text{-}H_2L)_2(\mu_3\text{-}OH)_2(\mu_{1,3}\text{-}O_2C\text{-}C_6H_4\text{-}p\text{-}NO_2)_2](ClO_4)(p\text{-}NO_2\text{-}C_6H_4\text{-}CO_2)\cdot DMF\cdot 5H_2O$ (**3**) and one dinuclear nickel(II)-based chain complex $\{[Ni_2(\mu\text{-}H_2L)(\mu_{1,3}\text{-}O_2CCH_2Ph)_2(H_2O)](ClO_4)\cdot 1/2(CH_3OH)\}_n$ (**4**). These were obtained via the reaction of $Ni(ClO_4)_2\cdot 6H_2O$ with H_3L [2,6-bis((2-(2-hydroxyethylamino)ethylimino)methyl)-4-methylphenol] and RCO_2Na (R = CH_3,C_2H_5, $p\text{-}NO_2C_6H_4$, and $PhCH_2$). This family of complexes is developed from $\{Ni_2(\mu\text{-}H_2L)\}^{3+}$ fragments following self-aggregation. The complexes were characterized by X-ray crystallography and magnetic measurements. The changes from acetate, propionate, and *p*-nitrobenzoate to phenylacetate groups resulted in two different types of coordination aggregation. These compounds are new examples of $[Ni_4]$ and $[Ni_2]_n$ complexes where organization of the building motifs are guided by the type of the carboxylate groups responsible for in-situ generation and utilization of HO^- bridges with alteration in the aggregation process within the same ligand environment. Studies on the magnetic behavior of the compounds reveal that the exchange coupling within **1**−**4** is predominantly antiferromagnetic in nature.

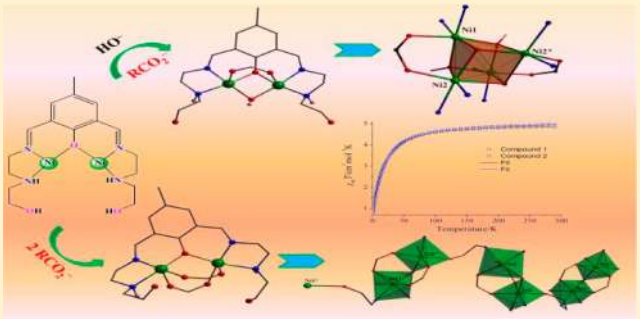

INTRODUCTION

Recent intense interest in the synthesis and characterization of high-nuclearity coordination cluster complexes of 3d metal ions is driven by a variety of reasons, such as their relevance to biologically significant structural motifs and to add new members to the ever growing family of magnetic materials.[1] Incorporation of nickel(II) ions within these from the coordination support of phenol-based ligands has been receiving increasing attention in recent years in the field of molecular magnetism and electronics.[2] The presence of nickel(II) ions is thus promising in the synthesis of both molecule-based magnets[3] and spin-phonon traps.[4,5]

Synthetic protocols for self-assembly reactions of building blocks within complex clusters often allow the isolation of a single thermodynamic product having high-order molecular architecture in high yield. Schiff bases are ideal candidates for supporting such cage structures due to the easy preparation procedure and easier handling of reaction conditions. Ancillary bridges work in collaboration with the primary ligand to stabilize the coordination assembly. A new family of phenol-bearing "dinucleating ligands", while simultaneously binding two nickel(II) ions, can be useful for the generation of Ni_2L-type building blocks. In the following step, depending upon the reaction condition and available ancillary bridges, these blocks can assemble into various molecular topologies, and the assembly process is sensitive to the nature of the side arms of the ligand backbone. Ancillary bridges such as HO^-, RO^-, and N_3^- are known to be crucial to support the cubane, defective dicubane, and other higher order topologies.[6] Until now numerous topologies have been reported, for example, cubane,[7a,b] open dicubane,[7c] stepped cubane,[7d] tetrahedron,[7e] and pentanuclear vertex-shared double cubane of hourglass type (Scheme S1 in the Supporting Information, SI).[8]

The utility of carboxylate ancillary bridges for coordination aggregates has been observed mainly for their linking potential in basal−apical positions around any square-pyramidal and distorted octahedral geometry. They connect via $\mu_{1,1}$ in syn-anti mode, $\mu_{1,3}$ in syn-syn, syn-anti, and anti-anti modes, $\mu_{1,1,3}$ in anti-syn-syn and anti-syn-anti modes, and $\mu_{1,1,3,3}$ in syn-anti-syn-anti mode.[9] From the viewpoint of their function as magnetic

Received: August 18, 2016
Published: September 29, 2016

DOI: 10.1021/acs.inorgchem.6b02015
Inorg. Chem. 2016, 55, 10783−10792

Chart I. Metal Binding Modes of Ligand H_3L

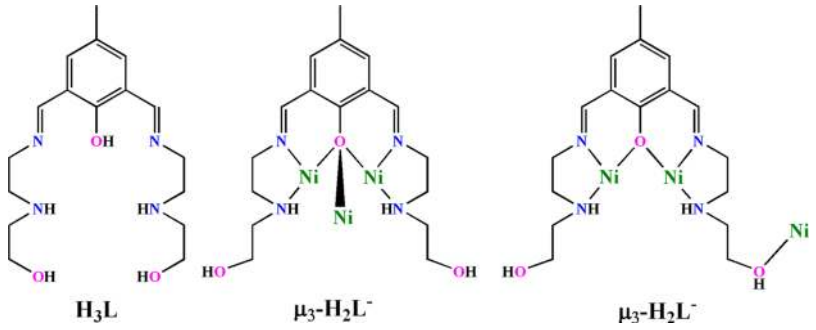

couplers, the syn-syn and anti-anti modes of binding result in antiferromagnetic interactions.

In the present course of work, we investigated the coordination behavior of a new Schiff base ligand H_3L (Chart I; 2,6-bis((2-(2-hydroxyethylamino)ethylimino)methyl)-4-methylphenol) toward nickel(II) ions in solution, followed by isolation of the products in the solid state. The ligand H_3L is new in coordination chemistry; only a group of $[Cu_6]$ complexes has been reported by our group with dumbbell-shaped topologies.[10] The bridging properties of carboxylate- and solvent-derived hydroxide groups (Scheme S2) have been exploited to stabilize cluster-like coordination aggregates. In the presence of carboxylate anions the Schiff base remains in the H_2L^- form and binds three nickel(II) ions in μ_3 forms.

Herein, we report two unique carboxylate coordination-driven self-organization reactions for the synthesis of three tetranuclear nickel(II) complexes $[Ni_4(\mu_3\text{-}H_2L)_2(\mu_3\text{-}OH)_2(\mu_{1,3}\text{-}O_2CR)_2]^{2+}$ [R = $-CH_3$, **1**; $-C_2H_5$, **2**; $-C_6H_4\text{-}NO_2$, **3**] and a polynuclear chain compound $\{[Ni_2(\mu\text{-}H_2L)(\mu_{1,3}\text{-}O_2CCH_2Ph)_2(H_2O)](ClO_4)\cdot 1/2(CH_3OH)\}_n$ (**4**) containing a different type of $\{Ni_2\}$ repeating unit bound to H_2L^-. The complexes have been isolated and crystallographically characterized, and their magnetic properties have been studied.

EXPERIMENTAL SECTION

Materials. The solvents and chemicals used in this work were obtained from commercial sources like SRL, India, Sigma-Aldrich, and Loba Chemie Laboratory Reagents & Fine Chemicals, India. Sources: Sodium acetate, propionic acid, and phenylacetic acid from SD Fine-chem Limited and *p*-nitrobenzoic acid from Alfa Aesar. The chemicals used in this work were reagent-grade materials and used as received without further purification. Nickel(II) perchlorate hexahydrate was freshly prepared by treating hydrated nickel(II) carbonate (11.89 g, 0.1 mol) with 1:1 aqueous solution of perchloric acid. Sodium propionate, sodium *p*-nitrobenzoate, and sodium phenylacetate were prepared by treating propionic acid (0.15 g, 2.0 mmol), *p*-nitrobenzoic acid (0.33 g, 2.0 mmol), and phenylacetic acid (0.27 g, 2.0 mmol) with sodium hydroxide (0.08 g, 2.0 mmol), followed by concentration and crystallization on a water bath. 2,6-Diformyl-4-methylphenol was synthesized following a literature procedure with modification providing better yield.[11]

Synthesis of Ligand H_3L [2,6-Bis{(2-(2-hydroxyethylamino)-ethylimino)methyl}-4-methylphenol]. To a MeOH solution (10 mL) of 2,6-diformyl-4-methylphenol (1.0 g, 6.1 mmol) in a round-bottom flask was added a MeOH solution (10 mL) of *N*-(hydroxyethyl)ethylenediamine (1.3 g, 12.2 mmol) dropwise with constant stirring. The mixture was then refluxed for 2 h over a heating mantle. After completion of the reaction, the solvent was removed from the reaction mixture by a rotatory evaporator, and H_3L was obtained as an orange oily mass. The ligand was characterized by FTIR, NMR, and ESI-MS spectroscopy and used directly for reaction without further purification.

FTIR (cm^{-1}, KBr disk): 3437(vs), 2981(w), 1637(s), 1054(w). ^1H NMR (600 MHz, $CDCl_3$, ppm): δ 8.23 (2H, imine-H), 6.80–6.60 (3H, Ar–H), 3.54 (2H, methylene CH_2), 3.83 (3H, methylene CH_2 attached with O atom), 1.30 (3H, methyl-H). ^{13}C NMR (101.4 MHz, $CDCl_3$, ppm): δ 162.23 (imine C), 157.01, 114.04, 70.71, 56.16, 50.94, 23.77. ESI-MS (MeOH solution, *m*/*z*): 251.14 ($C_{13}H_{19}N_2O_3$), 265.15 ($C_{12}H_{15}N_2Na_2O_2$), 165.05 ($C_9H_9O_3$), 399.19 ($C_{17}H_{29}N_4Na_2O_4$).

Complexes. A general method was used for preparation of all complexes. To a yellow MeOH (10 mL) solution of H_3L (0.36 g, 1.0 mmol) was added $Ni(ClO_4)_2\cdot 6H_2O$ (0.73 g, 2 mmol) with stirring at room temperature in air. After 15 min, aqueous solutions of the respective sodium carboxylates (2.0 mmol) were added to the previous reaction mixture. The whole reaction mixture was then stirred for 30 min and further refluxed for 1 h. The resulting clear reaction mixture was then cooled and filtered. The filtrate was then kept undisturbed for slow evaporation of solvent and growth of single crystals.

$[Ni_4(\mu_3\text{-}H_2L)_2(\mu_3\text{-}OH)_2(\mu_{1,3}\text{-}CH_3CO_2)_2](ClO_4)_2$ ***(1)***. Green single crystals suitable for X-ray structure analysis were obtained from the above-mentioned filtrate after 15 days. Yield: 0.48 g, 77%. Anal. Calcd for $C_{38}H_{58}Cl_2N_8Ni_4O_{20}$ (1252.58 g mol^{-1}): C, 36.44; H, 4.67; N, 8.95. Found: C, 35.75; H, 5.13; N, 8.69. Characteristic FTIR peaks (KBr, cm^{-1}; s = strong, vs = very strong, m = medium, br = broad): 3392(br), 1660(s), 1564(s), 1413(m), 1091(m), 626(m). Molar conductance, Λ_M (MeCN solution, Ω^{-1} cm^2 mol^{-1}): 154. UV–vis spectra [λ_{max}, nm (ε, L mol^{-1} cm^{-1})] (MeCN solution): 595 (42), 891 (52), 948 (32), 368 (8900).

$[Ni_4(\mu_3\text{-}H_2L)_2(\mu_3\text{-}OH)_2(\mu_{1,3}\text{-}C_2H_5CO_2)_2](ClO_4)_2\cdot 1/2H_2O$ ***(2)***. Light green single crystals suitable for X-ray analysis were obtained from the filtrate after 2 weeks. Yield: 0.92 g, 66%. Anal. Calcd for $C_{40}H_{67}Cl_2N_8Ni_4O_{20.5}$ (1293.14 g mol^{-1}): C, 34.74; H, 5.22; N, 8.66. Found: C, 35.24; H, 5.15; N, 7.88. FTIR peaks (KBr, cm^{-1}; s = strong, vs = very strong, m = medium, br = broad): 3421(br), 1654(s), 1560(s), 1411(m), 1089(m), 626(m). Molar conductance, Λ_M (MeCN solution, Ω^{-1} cm^2 mol^{-1}): 135. UV–vis spectra [λ_{max}, nm (ε, L mol^{-1} cm^{-1})] (MeCN solution): 588 (96), 891 (102), 954 (99), 368 (17 700).

$[Ni_4(\mu_3\text{-}H_2L)_2(\mu_3\text{-}OH)_2(\mu_{1,3}\text{-}CO_2\text{-}C_6H_4\text{-}NO_2)_2](ClO_4)(p\text{-}NO_2\text{-}C_6H_4\text{-}CO_2)\cdot DMF\cdot 5H_2O$ ***(3)***. On slow evaporation of the filtrate from the reaction mixture a green powder compound was obtained after 7 days. The obtained solid was then dissolved in DMF and allowed to crystallize. Green single crystals suitable for X-ray analysis were obtained after 2 weeks. Yield: 0.36 g, 42%. Anal. Calcd for $C_{58}H_{85}ClN_{12}Ni_4O_{30}$ (1699.91 g mol^{-1}): C, 40.96; H, 5.04; N, 9.88. Found: C, 40.75; H, 4.95; N, 9.76. Characteristic FTIR peaks (KBr, cm^{-1}; s = strong, vs = very strong, m = medium, br = broad): 3422(br), 1654(s), 1617(m), 1579(s), 1449 (m), 1400(m), 1343(s), 1091(m), 626(m). Molar conductance, Λ_M (MeCN solution, Ω^{-1} cm^2 mol^{-1}): 132. UV–vis spectra [λ_{max}, nm (ε, L mol^{-1} cm^{-1})] (MeCN solution): 597 (13), 366 (10 200).

$\{[Ni_2(\mu\text{-}H_2L)(\mu_{1,3}\text{-}O_2CCH_2Ph)_2(H_2O)](ClO_4)\cdot 1/2(CH_3OH)\}_n$ ***(4)***. Solvent evaporation from the filtrate gave green single crystals suitable for X-ray structure determination after 2 weeks. Yield: 0.63 g, 78%. Anal. Calcd for $C_{34}H_{47}ClN_4Ni_2O_{13}$ (872.21 g mol^{-1}): C, 46.80; H, 5.43; N, 6.42. Found: C, 46.71; H, 5.12; N, 6.20. Characteristic FTIR peaks (KBr, cm^{-1}; s = strong, vs = very strong, m = medium, br =

DOI: 10.1021/acs.inorgchem.6b02015
Inorg. Chem. 2016, 55, 10783–10792

Scheme 1. Synthetic Route for Complexes 1−4

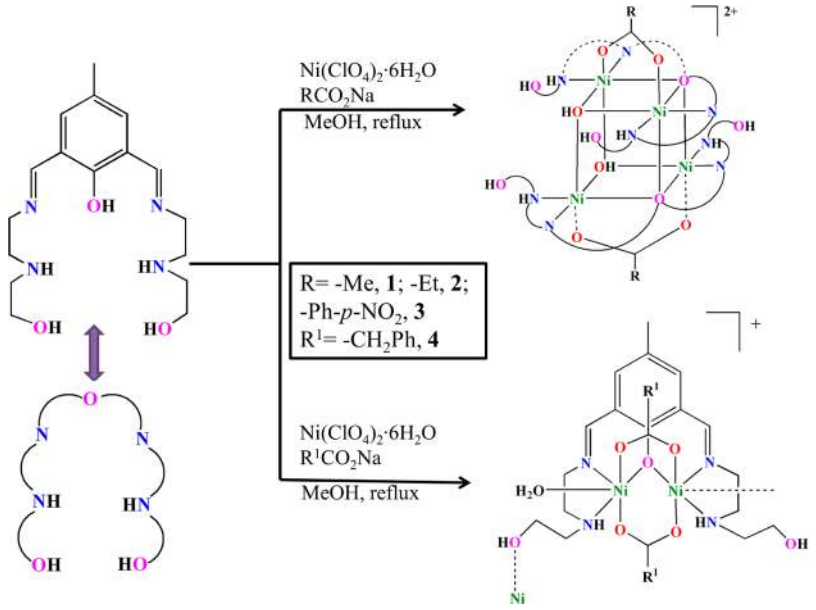

broad): 3378(br), 1655(s), 1578(s), 1422(m), 1099(s), 624(m). Molar conductance, Λ_M (MeCN solution, Ω^{-1} cm^2 mol^{-1}): 155. UV−vis spectra [λ_{max}, nm (ε, L mol^{-1} cm^{-1})] (MeCN solution): 579 (102), 892 (72), 947 (44), 387 (5700).

Caution! *Though we have not faced any problem while dealing with the title compounds, complexes of metal ions containing organic ligands along with perchlorate counteranions are explosive in nature. Therefore, it is safe to prepare a small amount of sample and handle it with care.*

Physical Measurements. Elemental analyses (C, H, and N) of the compounds were performed with a PerkinElmer model 240C elemental analyzer. A Shimadzu UV 3100 UV−vis−NIR spectrophotometer and a PerkinElmer RX1 spectrometer were used to record the solution electronic absorption spectra and FTIR spectra, respectively. The purity of the powder compounds was determined by powder X-ray diffraction (see SI) patterns using a Bruker AXS X-ray diffractometer (40 kV, 20 mA) using Cu Kα radiation (λ = 1.5418 Å) within a 5−50° (2θ) angular range and a fixed-time counting of 4 s at 25 °C.

Magnetic Measurements. Direct current (dc) magnetic measurements were performed on polycrystalline samples of compounds **1−4** constrained in eicosane using a Quantum Design SQUID magnetometer equipped with a 5 T magnet in the School of Chemistry at the University of Glasgow. The dc measurements were carried out in the temperature range 290−2.0 K under an applied field of 1000 Oe. Data were corrected for the diamagnetism of the compound through the approximation that $\chi_{DIA} \approx 0.5 \times MW \times 10^{-6}$ cm^3 mol^{-1} (MW = molecular weight) and for the diamagnetic contributions of the sample holder and eicosane through measurements.

Crystal Data Collection and Refinement. Suitable single crystals of **1−4** were chosen for X-ray diffraction. The data were collected on a Nonius Kappa CCD for **1** and a Bruker SMART APEX-II CCD diffractometer for **2−4** using a graphite-monochromated Mo Kα (λ = 0.71073 Å) radiation. The data were collected by ω scan (width of 0.3° frame^{-1}) method with a scan rate of 4 s per frame at 293 K for **1−3** and at 100 K for **4**. Data processing and space group determination were performed with SAINT and XPREP software.[12a] The structures were solved by direct method using SHELXS-97[12b] and refined with the SHELXL (2014/7)[12c] program package included into WINGX system Version 1.80.05.[12d] Data were corrected for Lorentz and polarization effects, and multiscan empirical absorption correction was applied using the SADABS program.[13] The locations of the heaviest atoms (Ni) were determined easily, and the difference Fourier maps were used to determine the position of O, N, and C. These atoms are refined anisotropically. The H atoms were incorporated at calculated positions and refined with fixed geometry and riding thermal parameters with respect to their carrier atoms. Crystallographic diagrams were prepared using DIAMOND software.[14] A summary of the crystal data and relevant refinement parameters is provided in Table S1. CCDC 1491624, 1491625, 1491626, and 1491627 contain the supplementary crystallographic data for complexes **1−4**.

RESULTS AND DISCUSSION

Synthetic Protocol. The Schiff base ligand 2,6-bis((2-(2-hydroxyethylamino)ethylimino)methyl)-4-methylphenol (H_3L) was prepared (Scheme S3) following a modified literature procedure,[15] and its reaction with nickel(II) perchlorate has been examined. The suitability of this ligand has been explored for the synthesis of multimetallic complexes. The reaction of $Ni(ClO_4)_2{\cdot}6H_2O$ with H_3L and different carboxylate salts [$(RCO_2)Na$, R = Me−, Et−, p-NO_2-Ph−, $PhCH_2$−] in MeOH in a 2:1:1 molar ratio led to formation of compounds **1−4** (Scheme 1).

Use of sodium acetate in a MeOH solution provided a brown reaction mixture from which green block-shaped crystals were isolated in 75% yield. The C, H, N analysis and single-crystal X-ray diffraction data (vide supra) confirm the formula for **1**. Conductivity measurement results are characteristic of 1:1 electrolyte which is in accordance with the presence of dinuclear fragments in solution state, confirmed from ESI-MS experiment (vide supra). The formation of **1** can be demonstrated by eq 1, which clearly justifies the suitability of CH_3COO^- ions to produce HO^- ions (vide infra, mass spectral analysis) to connect two nickel(II) ions initially in {$Ni_2(\mu$-$H_2L)(\mu$-OH)} fragments.

$$2H_3L + 4Ni(ClO_4)_2{\cdot}6H_2O + 6NaO_2CCH_3 \xrightarrow{MeOH} [Ni_4(\mu_3\text{-}OH)_2(\mu\text{-}H_2L)_2(\mu_{1,3}\text{-}O_2CCH_3)_2](ClO_4)_2 + 6NaClO_4 + 4HO_2CCH_3 + 22H_2O \quad (1)$$

We examined the reactivity pattern of other carboxylate salts keeping the molar ratio of the reagents unchanged with the hope to obtain a new family of Ni_4-based coordination aggregates. We were able to incorporate $C_2H_5CO_2^-$ and

DOI: 10.1021/acs.inorgchem.6b02015
Inorg. Chem. 2016, 55, 10783−10792

NO_2-$C_6H_4CO_2^-$ within the Ni_4-based clusters **2** and **3**, respectively. The reaction of $Ni(ClO_4)_2\cdot 6H_2O$ with H_3L and the respective carboxylate salts of sodium in a 2:1:1 molar ratio in MeOH led to the formation of **2** as green crystals and **3** as green powder from the reaction mixture in 66% and 42% yields. The formation of **2** and **3** can be summarized in eqs 2 and 3. The elemental analysis and molar conductivity data are consistent with the compositions for **2** and **3**, respectively. In the latter case, slow crystallization from DMF medium for a longer time period trapped both NO_2-$C_6H_4CO_2^-$ and ClO_4^- in the crystal lattice.

$$2H_3L + 4Ni(ClO_4)_2\cdot 6H_2O + 6NaO_2CC_2H_5 \xrightarrow{MeOH} [Ni_4(\mu_3\text{-}OH)_2(\mu\text{-}H_2L)_2(\mu_{1,3}\text{-}O_2CC_2H_5)_2](ClO_4)_2\cdot H_2O + 6NaClO_4 + 4HO_2CC_2H_5 + 21H_2O \quad (2)$$

$$2H_3L + 4Ni(ClO_4)_2\cdot 6H_2O + 6NaO_2CC_6H_4\text{-}NO_2 \xrightarrow{MeOH} [\text{Green powder}] \xrightarrow{DMF} [Ni_4(\mu_3\text{-}OH)_2(\mu\text{-}H_2L)_2(\mu_{1,3}\text{-}O_2CC_6H_4\text{-}NO_2)_2](ClO_4)(O_2CC_6H_4\text{-}NO_2)\cdot DMF\cdot 5H_2O \quad (3)$$

The reaction using the sodium salt of phenyl acetate did not lead to the generation of HO^- ions in situ for the μ-OH-based Ni_4 cubane formation. The reaction of H_3L with $Ni(ClO_4)_2$ in the presence of $PhCH_2CO_2Na$ in a 1:2:2 molar ratio led to the formation of green crystals of **4** in good yield according to eq 4. The use of phenyl acetate directs a different course of aggregation for interconnected Ni_4 units in a 1D chain arrangement. As a result, complex **4** is formed as a 1D chain through coordination of dangling alcohol arms.

$$nH_3L + 2nNi(ClO_4)_2\cdot 6H_2O + 2nNa(O_2CCH_2Ph) \xrightarrow{MeOH} \{[Ni_2(\mu\text{-}H_2L)(\mu_{1,3}\text{-}O_2CCH_2ph)_2(H_2O)](ClO_4)(H_2O)\}_n + 2nNaClO_4 + nHClO_4 + 11nH_2O \quad (4)$$

All four reactions in the presence of externally added bases like NEt_3, NaOMe, or NaOEt resulted in green gummy masses not suitable for thorough physical characterization.

FTIR Spectral Characterization. The presence of nickel(II)-bound alcohol arms, bridging HO− groups, and lattice water molecules in **1**−**4** is manifested by one broad band of medium intensity at 3392, 3421, 3422, and 3378 cm^{-1} and assigned to $\tilde{\nu}_{OH}$ stretching. Band broadening is observed due to extensive H-bonding interactions (Figure S1 in SI). The stretching vibrations of nickel(II)-bound imine bonds ($\tilde{\nu}_{C=N}$) are detected within 1654−1660 cm^{-1} for the four compounds. Examination of the carboxylate stretching frequencies helps us to identify the mode of bridging of the carboxylate moiety.[16] The asymmetric stretching vibration, $\tilde{\nu}_{as(COO)}$, of the carboxylate groups in **1**−**4** appears in the range of 1560−1579 cm^{-1}, while the symmetric stretching vibration $\tilde{\nu}_{s(COO)}$ is observed in the 1411−1449 cm^{-1} range. The difference, $\tilde{\nu}_{as(COO)} - \tilde{\nu}_{s(COO)} = \Delta\tilde{\nu}$, values (Table S4 in the SI) suggest a $\mu_{1,3}$-bridging mode for all carboxylate groups. Nonbridging monodentate carboxylate coordination to 3d metal ions leads to the observation of a greater magnitude of $\Delta\tilde{\nu}$ at ca. 250 cm^{-1}. The $\Delta\tilde{\nu}$ value for propionate is in good agreement with other reported values.[17] The noncoordinated NO_2-$C_6H_4CO_2^-$ counteranion in the lattice is confirmed from two medium-intensity peaks at 1617 ($\tilde{\nu}_{as(COO)}$) and 1400 cm^{-1} ($\tilde{\nu}_{s(COO)}$). The presence of a NO_2− group on the nickel(II)-bridged carboxylate function in **3** was observed as a strong peak at 1343 cm^{-1} due to a symmetric $\tilde{\nu}_{s(N-O)}$ stretching vibration.[18] Corresponding higher energy asymmetric stretching vibration modes of the NO_2 group appear within 1550−1500 cm^{-1} and merge with the carboxylate asymmetric stretching band. The perchlorate counteranions in T_d symmetry in all four complexes exhibits a strong band at ∼1090 cm^{-1} for $\nu_3(T_2)$ (ν_{ClO}) vibrational mode and a medium band at ∼624 cm^{-1} due to the $\nu_4(T_2)$ (δ_{dOClO}) vibrational modes.[19]

Powder X-ray Diffraction Patterns. The powder XRD patterns of the bulk materials of **1**−**4** were collected using a Bruker AXS X-ray diffractometer and compared with the simulated one derived from the single-crystal X-ray diffraction data. Figure S2 in the SI shows that the powder patterns are in good agreement with the simulated data. The difference in intensity is due to the orientation of the powder samples during the experiment. The similarity infers that the prepared powder samples are pure and have the exact composition of the single crystals.

Electronic Spectral Transitions. The appreciable solubility of the compounds in MeCN gave solutions suitable for identifying the electronic absorption bands in the 200−1200 nm range (Figure S3). Absorption bands with maxima (λ_{max}) at 595 (ε = 42 L mol^{-1} cm^{-1}), 588 (ε = 96 L mol^{-1} cm^{-1}), 597 (ε = 13 L mol^{-1} cm^{-1}), and 579 nm (ε = 102 L mol^{-1} cm^{-1}) for **1**, **2**, **3**, and **4**, respectively, can be assigned to spin-allowed $^3A_{2g}(F) \rightarrow {}^3T_{1g}(P)$ transitions consistent with the slightly distorted octahedral environments around the nickel(II) centers.[20] The $^3A_{2g}(F) \rightarrow {}^3T_{1g}(F)$ transitions were detected at 891 (ε = 52 L mol^{-1} cm^{-1}), 891 (ε = 102 L mol^{-1} cm^{-1}), and 892 nm (ε = 72 L mol^{-1} cm^{-1}), while the third and lowest energy $^3A_{2g}(F) \rightarrow {}^3T_{2g}(F)$ transition bands were located at 948 (ε = 32 L mol^{-1} cm^{-1}), 954 (ε = 99 L mol^{-1} cm^{-1}), and 947 nm (ε = 44 L mol^{-1} cm^{-1}) for **1**, **2**, and **4**, respectively. In the case of all four complexes, a very weak shoulder was observed near 730 nm for spin-forbidden $^3A_{2g}(F) \rightarrow {}^1E_g(F)$ electronic transition.[21] The $PhO^- \rightarrow$ Metal charge transfer transition (LMCT) band was observed at 368 (ε = 8900 L mol^{-1} cm^{-1}), 368 (ε = 17 700 L mol^{-1} cm^{-1}), 366 (ε = 10 200 L mol^{-1} cm^{-1}), and 387 nm (ε = 5700 L mol^{-1} cm^{-1}) for **1**, **2**, **3**, and **4**, respectively. The intense absorptions at ∼250 nm ($\varepsilon \approx$ 49 400 L mol^{-1} cm^{-1}) and shorter wavelength are due to intraligand $\pi \rightarrow \pi^*$ transitions.

Description of Crystal Structures. *$[Ni_4(\mu_3\text{-}H_2L)_2(\mu_3\text{-}OH)_2(\mu_{1,3}\text{-}CH_3CO_2)_2](ClO_4)_2$ (**1**), $[Ni_4(\mu_3\text{-}H_2L)_2(\mu_3\text{-}OH)_2(\mu_{1,3}\text{-}C_2H_5CO_2)_2](ClO_4)_2\cdot 1/2H_2O$ (**2**), and $[Ni_4(\mu_3\text{-}H_2L)_2(\mu_3\text{-}OH)_2(\mu_{1,3}\text{-}O_2C\text{-}C_6H_4\text{-}pNO_2)_2](ClO_4)(p\text{-}NO_2\text{-}C_6H_4\text{-}CO_2)\cdot DMF\cdot 5H_2O$ (**3**).* The molecular structure of the dicationic part of **1** is shown in Figure 1, and important bond lengths and angles are provided in Table S2 in the SI. The molecular structures of **2** and **3** are shown in Figure S4, and selected bond lengths and angles are listed in Table S2 in the SI. Both **1** and **2** crystallize in the tetragonal $I\bar{4}_{2d}$ space group, while **3** crystallizes in the monoclinic *Cc* space group. In the case of **1** and **2** the structures consist of a tetrametallic dicationic complex unit $[Ni_4(\mu_3\text{-}OH)_2(\mu_3\text{-}H_2L)_2(\mu_{1,3}\text{-}O_2CR)_2]^{2+}$ (RCO_2^-; R= $-CH_3$, $-C_2H_5$) and two perchlorate counteranions. In the case of **3**, the coordination cluster unit $[Ni_4(\mu_3\text{-}OH)_2(\mu_3\text{-}H_2L)_2(\mu_{1,3}\text{-}O_2C\text{-}C_6H_4\text{-}NO_2)_2]^{2+}$ is crystallized out by one perchlorate and one carboxylate group each as charge-neutralizing anions.

DOI: 10.1021/acs.inorgchem.6b02015
Inorg. Chem. 2016, 55, 10783−10792

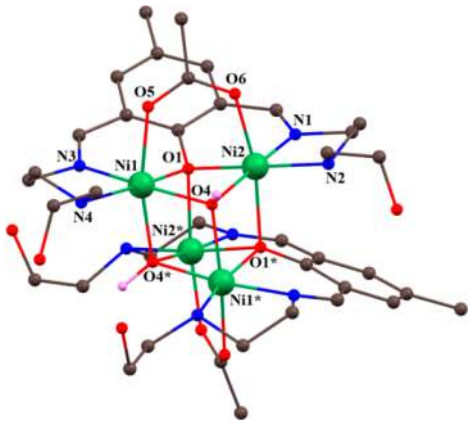

Figure 1. POV ray view of the $[Ni_4(\mu_3\text{-}H_2L)_2(\mu_3\text{-}OH)_2(\mu_{1,3}\text{-}O_2CMe)_2]^{2+}$ unit in **1** with partial atom-numbering scheme. Counteranions are omitted for clarity. H atoms are shown only for bridging −OH groups. Color code: Ni green, N blue, O red, C black, H pink.

The tetranuclear complex units consist of two monodeprotonated (only the phenol unit) ligands (H_2L^-), each of them delivering a set of N_4O donor atoms to the tetrametallic coordination cluster unit that organizes around two solvent water-derived μ_3-OH groups (O4 and O4*) located at the two corners of the distorted cube. The Ni···Ni separations vary from 2.958 to 3.216 Å (Table S2 in SI). The molecular structure of **1** can be assumed to grow from spontaneous aggregation of two $\{Ni_2(\mu\text{-}L)(\mu_2\text{-}OH)\}$ units, within which the phenoxido-hydroxido-bridged Ni1···Ni2 separation is shortest (2.9584 Å). Three faces are distinctly different due to the presence of capping carboxylates.

All four Ni^{II} ions remain in a distorted *octahedral* N_2O_4 coordination environment (Figure 2 and Figure S5 in the SI).

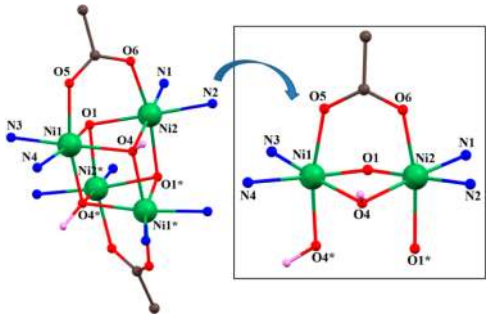

Figure 2. Core view of complex **1**, with partial atom-numbering scheme. (Inset) Asymmetric dinuclear unit.

The Ni−O distances vary within the 2.008−2.210 Å range versus the Ni−N distances at 2.001−2.116 Å. The phenoxido bridges tune the Ni−O−Ni angles within the cube in the 89.05−101.44° range, while the HO^- bridges record Ni−O−Ni angles in the 92.38−103.05° range. The double phenoxido-bridged face records the longest Ni···Ni distance of 3.317, 3.329, and 3.304 Å for **1**, **2**, and **3**, respectively, while the double hydroxido-bridged face has an intermediate separation of 3.216, 3.211, and 3.209 Å for **1**, **2**, and **3**, respectively.[22] The μ_3-phenoxido bridge supports, observed in **1**−**3**, for the growth of the cubes is exceptional in comparison to the μ_3-OH bridges. μ_3-OH and μ_3-OMe bridges most readily can use three available lone pairs to bind three different metal ions. As a result both hydroxido and methoxido groups can support cubane and dicubane structures quite readily. On the other hand, μ_3 bridging is not seen commonly with phenoxido ion. Only in a few cases it has been known for $[Ni_4]$ and $[Ni_6]$ complexes.[23] Within the Ni_4O_4 cube clusters the Ni^{II} centers in distorted *octahedral* geometry only help the formation of the cubic arrangement. On the other hand, tetrahedral O centers were responsible for the distortion in the cubic structure.

All three cationic complexes crystallize with perchlorate anions and water molecules. In the case of **1** and **2** the dangling hydroxyl groups of the ligand arms are engaged in intra- as well as intermolecular hydrogen-bonding interactions with each other. The perchlorate anions on the other hand establish hydrogen-bonding interactions with two μ_3-OH groups per Ni_4 cubane. Such connectivity results in hydrogen-bonded double-chain structures within the crystal lattice of **1** and **2**. The D···A distances range from 2.474 to 3.227 Å (Table S3), which confirms reasonably strong hydrogen-bonding interactions within the crystal lattice. Figure 3 and Figure S6 clearly describe the formation of H-bonded double-chain structures in **1** and **2**, respectively.

In the case of **3** strong hydrogen-bonding interactions between pendant alcohol arms of the ligand and available carboxylate anions are responsible for the partial substitution of perchlorate anions within crystal lattice. Lattice water molecules also take part in hydrogen-bond formation, reinforcing the supramolecular hydrogen-bonding interaction to stabilize the aggregate further (Figure 4). The D···A distances for all donors and acceptors involved in hydrogen-bonding range from 2.686 to 3.046 Å (Table S3), which confirms strong H-bonding interaction within the complexes. The D−H···A angles also fall in a wide range of 105−170°.

$\{[Ni_2(\mu\text{-}H_2L)(\mu_{1,3}\text{-}O_2CCH_2Ph)_2(H_2O)](ClO_4)\cdot 1/2(CH_3OH)\}_n$ (**4**). Complex **4** crystallizes in the monoclinic $P2_1/c$ space group, and the asymmetric unit contains a ligand-bound dinuclear fragment $[Ni_2(\mu\text{-}H_2L)(\mu_{1,3}\text{-}O_2CCH_2Ph)_2(H_2O)]^+$. The molecular structure of **4** is shown in Figure 5, and selected bond lengths and angles are listed in Table S2. Compound **4** has a 1D coordination polymeric structure based on $[Ni_2(\mu\text{-}H_2L)(\mu_{1,3}\text{-}O_2CCH_2Ph)_2]^+$ repeating units. The use of $PhCH_2CO_2^-$ ions in the reaction medium did not generate HO^- ions in good number to bridge two nickel(II) ions in comparison to $PhCH_2CO_2^-$ ions. This is also matching with the least basic nature of the phenylacetate moiety among all four carboxylates used in this study. Coordination of carboxylate modulates the structure of the $\{Ni_2(H_2L)\}$ fragment and fixes the position of the H_2L^- bridging hydroxido ion, which in turn helps in the organization of $\{Ni_2\}$ fragments for the product.

The asymmetric units are linked through the coordination of a dangling alcohol −OH group of one end of a nickel(II)-bound H_2L^- unit to one of the nickel(II) ions of the next unit. The distorted octahedral coordination geometry around two nickel(II) ions is shown in Figure 6.

The repeating $\{Ni_2\}$ fragment consists of one singly deprotonated H_2L^- ligand providing a set of N_4O_2 donor atoms, two carboxylate bridges, and one coordinated water molecule. These $\{Ni_2\}$ units are very loosely bridged by the oxygen atom (O2*) of a dangling alcohol arm of the adjacent unit. The Ni−O distances in the 2.016−2.174 Å range are close to the Ni−N separations at 1.985−2.210 Å. The Ni−O(H) bond distance is 2.160 Å, while the Ni−Ow is the longest and has a bond length of 2.174 Å. The distorted octahedral environments around each Ni^{II} ion are reflected in the variation

DOI: 10.1021/acs.inorgchem.6b02015
Inorg. Chem. 2016, 55, 10783−10792

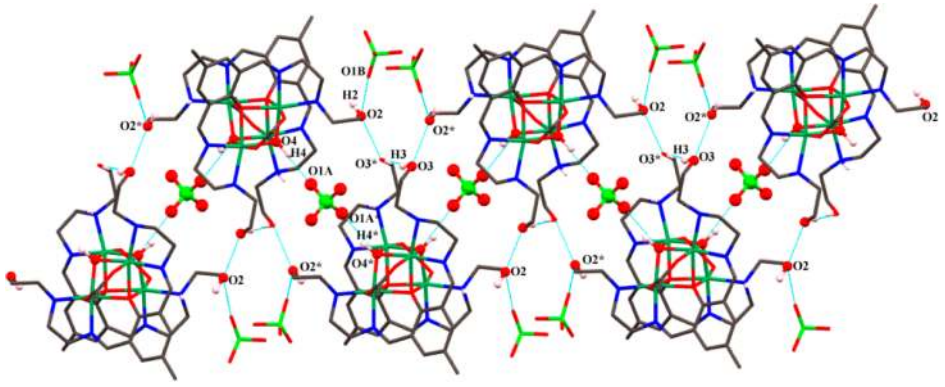

Figure 3. H-bonded double-chain formation in complex **1**.

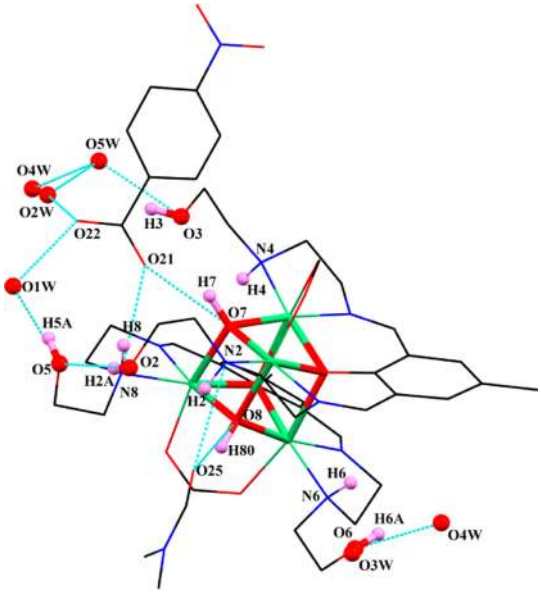

Figure 4. H-bonded aggregation in **3**.

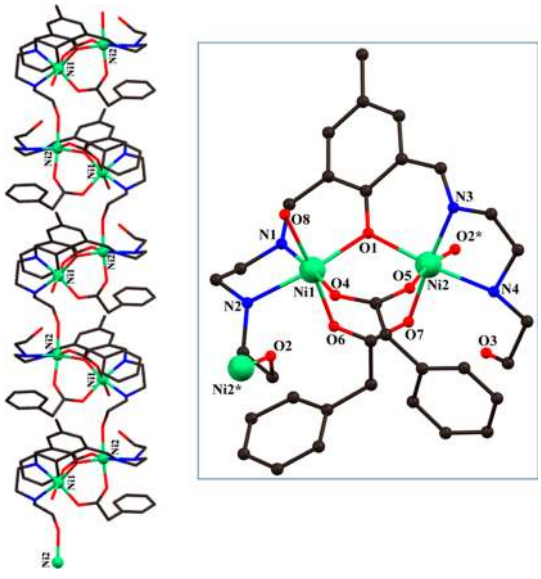

Figure 5. POV ray view of the cationic 1D chain (left) and dinuclear repeating unit $[Ni_2(\mu\text{-}H_2L)(\mu_{1,3}\text{-}O_2CCH_2Ph)_2]^+$ in **4** with partial atom-numbering scheme. Counteranions and H atoms are omitted for clarity. Color code: Ni green, N blue, O red, C black.

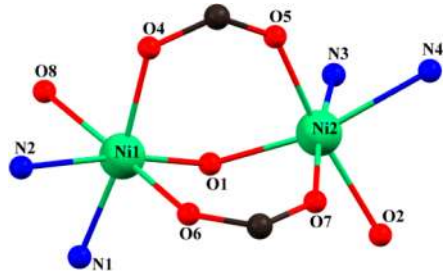

Figure 6. Octahedral environments of two nickel(II) centers within the asymmetric unit of **4**. Color code: Ni green, N blue, O red, C black.

of the cis and trans angles in the 79.4−99.7° and 169.5−174.3° ranges. The phenoxido (O1) and double carboxylato-bridged Ni···Ni distance is 3.435 Å, whereas the Ni···Ni separation within interdimeric units is in the 5.704−8.840 Å range (Figure 7).

Intramolecular hydrogen-bonding interactions further stabilize the weak interdinuclear link formed from alcoholic HO− coordination (Figure S7). Both the nickel(II)-bound −OH group (O2) and the dangling −OH arm (O3) within the $\{Ni_2(H_2L)\}$ fragment are hydrogen bonded to the O donors (O4 and O7) of bound carboxylates and one −NH (N2) group of another $\{Ni_2(H_2L)\}$ unit. Characteristic hydrogen-bonding parameters are listed in Table S3 in SI.

Mass Spectroscopic Identification of the Fragments. The existence of different $\{Ni_2(H_2L)\}$-based key fragments in solution were established from mass spectral (ESI-MS positive) analysis of compounds **1**−**4** in MeOH solutions (Figure S8−S11). Aggregation of these fragments resulted in the products during synthesis and crystallization in the solid state.

Complex 1: In the spectra of **1** in MeOH solution two intense peaks were obtained at m/z = 449.06 (calcd 449.06) and 499.06 (calcd 499.10) which can be attributed to the $[Ni_2L]^+$ ($C_{17}H_{25}N_4Ni_2O_3$) and $[Ni_2(HL)(OH)(CH_3OH)]^+$ ($C_{18}H_{31}N_4Ni_2O_5$) fragments, respectively. The medium-intensity peak observed at m/z = 549.02 (calcd 549.01) can be assigned to the fragment $[Ni_2(HL)(ClO_4)]^+$ ($C_{17}H_{26}ClN_4Ni_2O_7$). ESI-MS showed no evidence in support of a $[Ni_4]$ aggregate in the solution phase. The acetate-bound $\{Ni_2\}$ fragment produced in solution is manifested by a small peak at m/z = 650.97 (calcd 649.03) of molecular formula $[Ni_2(H_2L)(OH)(O_2CCH_3)\text{-}Na]^+$ ($C_{19}H_{31}ClN_4NaNi_2O_{10}$). During crystallization two such fragments collapse to yield **1** as crystals from solution.

DOI: 10.1021/acs.inorgchem.6b02015
Inorg. Chem. 2016, 55, 10783−10792

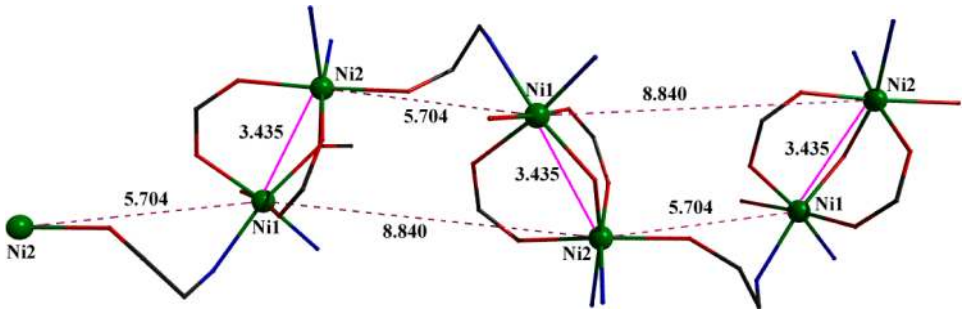

Figure 7. POV ray view of the 1D coordination chain containing a Ni_4 repeating unit in **4** showing Ni···Ni separation (in Angstroms).

Complex 2: In this case the peaks at 449.06 and 549.02 for molecular fragments $[Ni_2L]^+$ and $[Ni_2(HL)(ClO_4)]^+$ are also present in the ESI-MS spectrum of **2** in MeOH. The base peak at m/z = 307.05 (calcd 307.06) can be assigned to the hydrolyzed ligand part in the molecular fragment $[Ni(HL')]^+$ ($C_{13}H_{17}N_2NiO_3$). The presence of a monocationic $\{Ni_2\}$ fragment $[Ni_2(H_2L)(ClO_4)(O_2CC_2H_5)]^+$ ($C_{20}H_{32}ClN_4Ni_2O_9$) in solution phase, characteristic for bound $C_2H_5CO_2^-$, originating from **2** is confirmed by a medium-intensity peak at m/z = 623.10 (calcd 623.05).

Complex 3: All previously mentioned peaks at m/z = 449.06, 499.06, and 549.02 for $[Ni_2L]^+$, $[Ni_2(HL)(OH)(CH_3OH)]^+$, and $[Ni_2(HL)(ClO_4)]^+$ fragments are present in the ESI-MS spectrum of **3** in MeOH. Additionally, the most characteristic *p*-nitrobenzoate-bound $\{Ni_2\}$ distinguishing fragment $[Ni_2(HL)(p\text{-}NO_2\text{-}C_6H_4\text{-}CO_2)]^+$ ($C_{24}H_{30}N_5Ni_2O_7$) in **3** has been identified by a medium-intensity peak in the ESI-MS spectrum at m/z = 616.08 (calcd 616.09).

Complex 4: Along with the common peaks at m/z = 449.06 and 549.02 in the ESI-MS of **4**, the obtained distinctive and medium-intensity peak at m/z = 307.06 can be assigned to the mononuclear nickel(II)-bound hydrolyzed ligand fragment $[Ni(HL')]^+$ ($C_{13}H_{17}N_2NiO_3$). Dissolution of **4** in MeOH resulted in the solution-stable monophenylacetate-bound dinuclear fragment $[Ni_2(HL)(O_2CCH_2Ph)]^+$ ($C_{25}H_{33}N_4Ni_2O_5$) and bis-phenylacetate-bound fragment $[Ni_2(H_2L)(O_2CCH_2Ph)_2]^+$ ($C_{33}H_{41}N_4Ni_2O_7$) corresponding to the characteristic peaks at m/z = 585.12 (calcd 585.11) and 721.17 (calcd 721.16) in the ESI-MS spectrum.

The mass spectral (ESI-MS positive) evidence thus established the self-aggregation of dimeric fragments in one way for production of **1**−**3** and the polymeric nickel complex **4** via a different route.

Magnetic Studies. The temperature dependence of the molar magnetic susceptibility, χ_M, of compounds **1**−**4** was measured under a magnetic field of 0.1 T over the temperature range 290−2 K. Figure 8 shows the plots of $\chi_M T$ versus temperature, T, for compounds **1** and **2** (compound **3** is omitted for clarity and shown in Figure S12 in the SI). At 290 K, the values of $\chi_M T$ are 4.86, 4.96, and 5.13 $cm^3\ mol^{-1}\ K$ for **1**, **2**, and **3**, respectively, which are all in line with expected values for four uncoupled Ni^{II} ions with $g \approx 2.2$ within these multimetallic assemblies. On decreasing the temperature, **1**−**3** show a continual decrease in the value of $\chi_M T$, which may be caused by predominant antiferromagnetic exchange interactions between the Ni^{II} ions but also by zero-field splitting (zfs) and antiferromagnetic intermolecular interactions at low temperature.

These data were fitted with the program Phi 2.0.[24] The asymmetric nature of the cubanes means that they require four

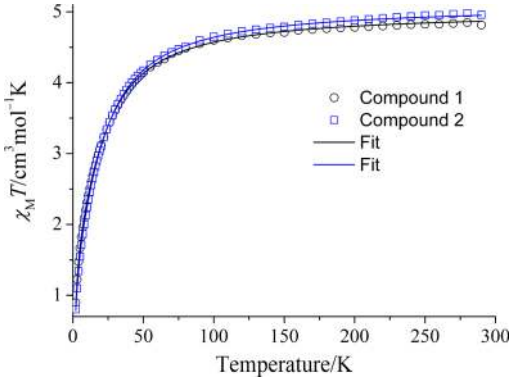

Figure 8. Plot of $\chi_M T$ vs T for **1** and **2**. Solid lines represent fits of the data as described in the text.

different exchange interactions to be considered; Figure 9 illustrates the different faces found in compound **1**. For **1**−**3**,

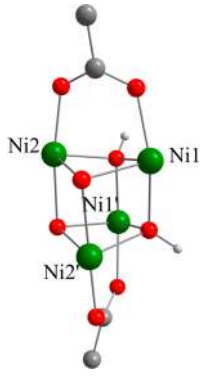

Figure 9. View of the cubane core in **1**, highlighting the different types of bridge on each face as described in the text.

the top and bottom faces of the distorted cubane were taken as those capped by the *syn*,*syn*-carboxylate groups and correspond to J_1 between Ni1 and Ni2 and Ni1′ and Ni2′; the two lateral, opposing faces bridged by one hydroxyl group and a phenoxy oxygen atom are represented by J_2 between Ni1 and Ni2′ and Ni2 and Ni1′. The coupling constant J_3 corresponds to the face bridged by two phenoxido O atoms, mediating the interaction between Ni2 and Ni2′, and J_4 corresponds to the pathway between Ni1 and Ni1′, which are bridged by two hydroxido groups. The same bridges and cubane faces are found in each complex and represented by the same coupling constant, but the exact label for the Ni^{II} ions depends on the crystallographic symmetry. To avoid overparameterization of the fit, the g values were fixed, while the possible contribution from zfs associated

DOI: 10.1021/acs.inorgchem.6b02015
Inorg. Chem. 2016, 55, 10783−10792

with the Ni^{II} ions was neglected. The Hamiltonian employed was

$$\hat{H} = -2J_1(\hat{S}_{Ni1}\hat{S}_{Ni2} + \hat{S}_{Ni1'}\hat{S}_{Ni2'}) - 2J_2(\hat{S}_{Ni1}\hat{S}_{Ni2'} + \hat{S}_{Ni1'}\hat{S}_{Ni2}) - 2J_3(\hat{S}_{Ni2}\hat{S}_{Ni2'}) - 2J_4(\hat{S}_{Ni1}\hat{S}_{Ni1'}) + g\mu_B H\sum_{i=1}^{4}\hat{S}_i$$

The $\chi_M T$ curves resulting from these fits are shown in Figure 8, and the derived parameters are given in Table 1.

Table 1. Summary of the Exchange Interactions Derived from the Fits of the Magnetic Data for 1−3

complex	g	J_1 (cm^{-1})	J_2 (cm^{-1})	J_3 (cm^{-1})	J_4 (cm^{-1})
1	2.24	−2.03	+0.98	+0.32	−7.31
2	2.26	−2.58	+1.21	+0.70	−7.26
3	2.27	−2.03	+1.30	+0.04	−6.78

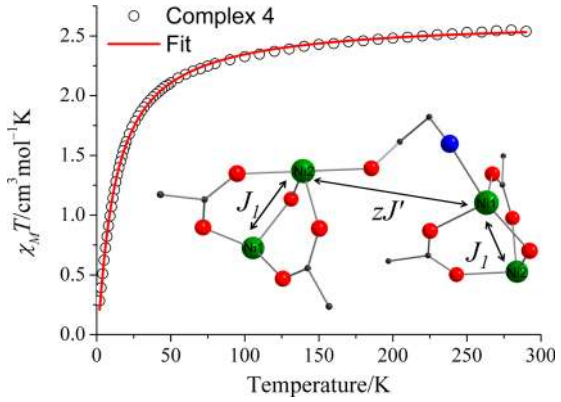

Figure 10. Plot of $\chi_M T$ vs T for **4**. Solid red line corresponds to the fit of the data described in the text. (Inset) Topology used for the exchange interactions.

Previous magneto-structural correlations have shown that the average Ni−O−Ni angle is one of the most important parameters in deciding the nature and strength of the exchange coupling interactions mediated across the faces of a cubane.[25] At angles of approximately 99°, the exchange interaction between Ni^{II} ions changes sign, with angles closer to 90° leading to stronger ferromagnetic coupling, while angles above 100° lead to antiferromagnetic coupling. Broadly, this trend is observed in compounds **1**−**3** (Table 1), where the interaction across the largest average Ni−O−Ni angle, J_4 [101.8(3)° in **1**, 101.9(2)° in **2**, and 102.5(3)° in **3**], leads to the strongest antiferromagnetic coupling interaction between the Ni^{II} ions. The exchange across the faces with average Ni−O−Ni angles that lie close to 99° is weaker [98.2(1)° in **1**, 97.9(1)° in **2**, and 98.5(1)° in **3**] and found to be ferromagnetic in all three cases. An exception to this correlation is provided by the interactions across the carboxylate-capped faces, which are found to be antiferromagnetic despite the average Ni−O−Ni angles for all three compounds lying close to 90° [91.1(1)°, 90.9(1)°, and 91.6(1)° for **1**, **2**, and **3**, respectively]. However, the correlation established is considered[26] in only those cubanes that were bridged by μ_3-OR groups (RO = hydroxido, methoxido, alkoxido, and phenoxido) and ignored those containing a secondary bridge such as carboxylate groups. Other previous papers have found the presence of *syn,syn*-carboxylate bridges to result in strong deviations from the coupling anticipated based on magneto-structural correlations, often favoring antiferromagnetic exchange.[20,27]

Figure 10 displays the plot of $\chi_M T$ versus temperature, T, for compound **4**. The room-temperature value of $\chi_M T$ = 2.53 cm^3 mol^{-1} K is in line with that expected for two uncoupled Ni^{II} ions with $g \approx 2.25$. To fit the magnetic data with Phi 2.0, compound **4** was considered as discrete dinuclear units that are linked together into a chain. One coupling constant was considered between the Ni1 and the Ni2 ions (J_1), and the interaction between the neighboring dimers and chains was introduced as an intermolecular interaction (zJ'). As with compounds **1**−**3**, the g factors were assumed to be the same for each Ni^{II} ion, and any zfs associated with the Ni^{II} ions was neglected. The results of the fit yielded g = 2.29, J_1 = −1.56 cm^{-1}, and zJ' = −0.93 cm^{-1}. The g value and strength of the antiferromagnetic coupling are in line with those previously observed for other comparable, triply bridged, dinuclear Ni^{II} units.[28] Due to the model employed, the intermolecular interaction is larger than expected, because it takes into account intrachain interactions between dinuclear units, as well as any possible interchain interactions and any decrease in $\chi_M T$ caused by zfs.

CONCLUSIONS

Utilization of the coordination potential of 2,6-bis[{2-(2-hydroxyethylamino)ethylimino}methyl]-4-methylphenol with nickel(II) perchlorate and aggregation propensity of the fragments thus formed have been studied in this work. In the presence of four different carboxylates these fragments led to the generation and isolation of two types of self-organized aggregates depending on the nature and number of bound carboxylate anions. The use of acetate, propionate, and *p*-nitrobenzoate to phenylacetate groups in the reaction medium resulted in two distinct courses of aggregation reactions. In one case, three $[Ni_4]$ coordination clusters have been grown from in-situ trapping of HO^- ions from H_2O of the reaction medium. In the other case, use of phenylacetate bridges provided a $[Ni_2]_n$ chain complex through linking of $\{Ni_2(\mu\text{-}H_2L)\}^{3+}$ units by dangling alcohol arms of the ligands. In the reaction medium H_2L^- was used initially to trap two Ni^{II} ions, leaving behind available coordinating sites for hydroxide and carboxylate binding followed by assembly of two or more ligand-bound $\{Ni_2(\mu\text{-}H_2L)\}^{3+}$ units for tetrameric $[Ni_4]$ and interconnected $[Ni_2]_n$ complex formation. Two solvent-derived HO^- groups present in one face of the $[Ni_4]$ distorted cube do bring Ni···Ni separations within 2.958−3.216 Å, whereas in the case of the polynuclear 1D chain the phenoxido and double carboxylato bridges result in shorter Ni···Ni separations of 3.435 Å, which is considerably shorter than the Ni···Ni separation within interdimeric units at 5.704−8.840 Å. In three of the discrete $[Ni_4]$ complexes the face-wise dependence of Ni−O−Ni angles for ferromagnetic and antiferromagnetic interactions was observed. In the case of complex **4**, the single important coupling constant (J_1) was found to be antiferromagnetic in nature with a small value of −1.56 cm^{-1}. As a continuation of the work, we are exploring the bridging potential of in-situ-derived carbonate and externally available nitrate, cyanate, oxalate, sulfide, thiocyanate, peroxide, and azide ions systematically in this reaction protocol to obtain other types of self-assembled and interlinked $[Ni_2]$ aggregates.

DOI: 10.1021/acs.inorgchem.6b02015
Inorg. Chem. 2016, 55, 10783−10792

■ ASSOCIATED CONTENT

Supporting Information

The Supporting Information is available free of charge on the ACS Publications website at DOI: 10.1021/acs.inorgchem.6b02015.

Topologies of nickel complexes known in the literature, metal binding modes of ancillary ligands, formation of H_3L, FTIR spectra of **1**−**4**, comparative powder XRD patterns of **1**−**4**, charge transfer and d−d transition bands for **1**−**4**, POV ray representation for $[Ni_4(H_2L)_2(\mu_3\text{-}OH)_2(\mu_{1,3}\text{-}O_2CEt)_2]^{2+}$ unit in **2** and $[Ni_4(H_2L)_2(\mu_3\text{-}OH)_2(\mu_{1,3}\text{-}O_2C\text{-}C_6H_4\text{-}NO_2)_2]^{2+}$ unit in **3** with partial atom-numbering scheme, core structures of **2** and **3**, H-bonded double-chain formation within **2**, intramolecular H bonding within 1D coordination polymer **4**, ESI MS spectra of **1** in MeOH, ESI MS spectra of **2** in MeOH, ESI MS spectra of **3** in MeOH, ESI MS spectra of **4** in MeOH, $\chi_M T$ versus T plot for **3**, crystal data and structure refinement details for compounds **1**−**4**, selected bond distances and bond angles for **1**−**4**, hydrogen-bonding parameters for **1**−**4**, and carboxylate stretching frequencies of complexes **1**−**4** (PDF)

X-ray crystallographic data (ZIP)

■ AUTHOR INFORMATION

Corresponding Author

*E-mail: dray@chem.iitkgp.ernet.in. Phone: (+91) 3222-283324. Fax: (+91) 3222-82252.

Notes

The authors declare no competing financial interest.

■ ACKNOWLEDGMENTS

K.C. is thankful to the Council of Scientific and Industrial Research, New Delhi, for financial support. We are also thankful to DST, New Delhi, for providing the Single Crystal X-ray Diffractometer facility to the Department of Chemistry, IIT Kharagpur, under its FIST program. The UK Engineering and Physical Sciences Research Council is thanked for financial support (grant ref EP/K033662/1).

■ REFERENCES

(1) (a) Aubin, S. M.; Dilley, N. R.; Pardi, L.; Krzystek, J.; Wemple, M. W.; Christou, G.; Hendrickson, D. N. Resonant magnetization tunneling in the trigonal pyramidal $Mn^{IV}Mn^{III}_3$ complex $[Mn_4O_3Cl(O_2CCH_3)_3(dbm)_3]$. *J. Am. Chem. Soc.* **1998**, *120* (20), 4991−5004. (b) Gatteschi, D.; Sessoli, R. Quantum tunneling of magnetization and related phenomena in molecular materials. *Angew. Chem., Int. Ed.* **2003**, *42* (3), 268−297. (c) Chen, S. Y.; Beedle, C. C.; Gan, P. R.; Lee, G. H.; Hill, S.; Yang, E. C. Half-integer spin heptanuclear single-molecule magnet with an unusual $Mn^{III}_6Mn^{II}$ exchange-coupled core. *Inorg. Chem.* **2012**, *51* (8), 4448−4457. (d) Figuerola, A.; Tangoulis, V.; Ribas, J.; Hartl, H.; Brüdgam, I.; Maestro, M.; Diaz, C. Synthesis, crystal structure, and magnetic studies of oxo-centered trinuclear chromium (III) complexes:$[Cr_3(\mu_3\text{-}O)(\mu_2\text{-}PhCOO)_6(H_2O)_3]NO_3\cdot 4H_2O\cdot 2CH_3OH$, a case of spin-frustrated system, and $[Cr_3(\mu_3\text{-}O)(\mu_2\text{-}PhCOO)_2(\mu_2\text{-}OCH_2CH_3)_2(bpy)_2(NCS)_3]$, a new type of $[Cr_3O]$ core. *Inorg. Chem.* **2007**, *46* (26), 11017−11024.

(2) (a) Hazra, S.; Koner, R.; Lemoine, P.; Sañudo, E.; Mohanta, S. Syntheses, structures and magnetic properties of heterobridged dinuclear and cubane-type tetranuclear complexes of nickel(II) derived from a Schiff base ligand. *Eur. J. Inorg. Chem.* **2009**, *2009*, 3458−3466. (b) Lu, Z.; Fan, T.; Guo, W.; Lu, J.; Fan, C. Synthesis, structure and magnetism of three cubane Cu (II) and Ni (II) complexes based on flexible Schiff-base ligands. *Inorg. Chim. Acta* **2013**, *400*, 191−196.

(3) Milios, C. J.; Winpenny, R. E. P. Cluster-based single-molecule magnets. *Struct. Bonding (Berlin, Ger.)* **2014**, *164*, 1−119.

(4) Carretta, S.; Santini, P.; Amoretti, G.; Affronte, M.; Candini, A.; Ghirri, A.; Tidmarsh, I. S.; Laye, R. H.; Shaw, R.; McInnes, E. J. L. High-temperature slow relaxation of the magnetization in Ni_{10} magnetic molecules. *Phys. Rev. Lett.* **2006**, *97*, 207201.

(5) Krzystek, J.; Telser, J.; Pardi, L. A.; Goldberg, D. P.; Hoffman, B. M.; Brunel, L.-C. High-frequency and-field electron paramagnetic resonance of high-spin manganese (III) in porphyrinic complexes. *Inorg. Chem.* **1999**, *38*, 6121−6129.

(6) (a) Gao, Y. Z.; Zhang, Y. A.; Zhang, J. Synthesis, structures, and magnetic properties of tetranuclear nickel and cobalt complexes with 2-mercaptobenzoxazole. *Inorg. Chem. Commun.* **2015**, *54*, 85−88. (b) Reger, D. L.; Pascui, A. E.; Pellechia, P. J.; Smith, M. D.; Jezierska, J.; Ozarowski, A. Hydroxide-bridged cubane complexes of nickel (II) and cadmium (II): magnetic, EPR, and unusual dynamic properties. *Inorg. Chem.* **2014**, *53*, 4325−4339.

(7) (a) Sieber, A.; Boskovic, C.; Bircher, R.; Waldmann, O.; Ochsenbein, S. T.; Chaboussant, G.; Güdel, H. U.; Kirchner, N.; van Slageren, J.; Wernsdorfer, W.; Neels, A.; Stoeckli-Evans, H.; Janssen, S.; Juranyi, F.; Mutka, H. Synthesis and spectroscopic characterization of a new family of Ni_4 spin clusters. *Inorg. Chem.* **2005**, *44*, 4315−4325. (b) Mandal, D.; Hong, C. S.; Kim, H. C.; Fun, H.-K.; Ray, D. A new $[Ni^{II}_4]$ distorted cubane assembly on four solvent derived μ_3−OMe corners: Solvent dependent formation and cleavage of exogenous bridges. *Polyhedron* **2008**, *27*, 2372−2378. (c) Liu, S.; Wang, S.; Cao, F.; Fu, H.; Li, D.; Dou, J. Crystallization condition-controlled assembly of oxygen-bridged tetranuclear and hexanuclear Ni(II) clusters: syntheses, structures and properties. *RSC Adv.* **2012**, *2*, 1310−1313. (d) Tandon, S. S.; Bunge, S. D.; Rakosi, R.; Xu, Z.; Thompson, L. K. Self-assembly of mixed-valence Co(II/III) and Ni(II) clusters: azide-bridged 1D single chain coordination polymers comprised of tetranuclear units, tetranuclear Co(II/III) complexes, ferromagnetically coupled azide-bridged tetranuclear, and hexanuclear Ni(II) complexes: synthesis, structural, and magnetic properties. *Dalton Trans.* **2009**, 6536−6551. (e) Sarkar, M.; Clérac, R.; Mathonière, C.; Hearns, N. G. R.; Bertolasi, V.; Ray, D. New μ_4-oxido-bridged copper benzoate quasi-tetrahedron and bis-μ_3-hydroxido-bridged copper azide and copper thiocyanate stepped cubanes: core conversion, structural diversity, and magnetic properties. *Inorg. Chem.* **2010**, *49*, 6575−6585.

(8) (a) Papatriantafyllopoulou, C.; Stamatatos, T. C.; Wernsdorfer, W.; Teat, S. J.; Tasiopoulos, A. J.; Escuer, A.; Perlepes, S. P. Combining azide, carboxylate, and 2-pyridyloximate ligands in transition-metal chemistry: Ferromagnetic Ni^{II}_5 clusters with a bowtie skeleton. *Inorg. Chem.* **2010**, *49*, 10486−10496. (b) Ghosh, A. K.; Shatruk, M.; Bertolasi, V.; Pramanik, K.; Ray, D. Self-assembled tetra- and pentanuclear nickel(II) aggregates from phenoxido-based ligand-bound $\{Ni_2\}$ fragments: Carboxylate bridge controlled structures. *Inorg. Chem.* **2013**, *52*, 13894−13903.

(9) (a) Mukherjee, S.; Weyhermüller, T.; Bothe, E.; Wieghardt, K.; Chaudhuri, P. Single-atom O-bridged urea in a dinickel(II) complex together with Ni^{II}_4, Cu^{II}_2 and Cu^{II}_4 complexes of a pentadentate phenol-containing Schiff base with (O, N, O, N, O)-donor atoms. *Eur. J. Inorg. Chem.* **2003**, *2003*, 863−875. (b) Colacio, E.; Domínguez-Vera, J. M.; Ghazi, M.; Kivekäs, R.; Klinga, M.; Moreno, J. M. Singly *anti-anti* carboxylate-bridged zig-zag chain complexes from a carboxylate-containing tridentate Schiff base ligand and $M(hfac)_2$ [M = Mn^{II}, Ni^{II}, and Cu^{II}]: Synthesis, crystal structure, and magnetic properties. *Eur. J. Inorg. Chem.* **1999**, *1999*, 441−445. (c) Cañadillas-Delgado, L.; Fabelo, O.; Pasán, J.; Delgado, F. S.; Lloret, F.; Julve, M.; Ruiz-Pérez, C. Unusual (μ-aqua)bis(μ-carboxylate) bridge in homometallic M(II) (M = Mn, Co and Ni) two-dimensional compounds based on the 1,2,3,4-butanetetracarboxylic acid: Synthesis, structure, and magnetic properties. *Inorg. Chem.* **2007**, *46* (18), 7458−7465.

(10) Chattopadhyay, K.; Shaw, B. K.; Saha, S. K.; Ray, D. *Dalton Trans.* **2016**, *45*, 6928−6938.

DOI: 10.1021/acs.inorgchem.6b02015
Inorg. Chem. 2016, 55, 10783−10792

(11) Gagne, R. R.; Spiro, C. L.; Smith, T. J.; Hamann, C. A.; Thies, W. R.; Shiemke, A. K. The synthesis, redox properties, and ligand binding of heterobinuclear transition-metal macrocyclic ligand complexes. Measurement of an apparent delocalization energy in a mixed-valent copper (I) copper (II) complex. *J. Am. Chem. Soc.* **1981**, *103*, 4073−4081.
(12) (a) *SAINT, SMART and XPREP*, Siemens Analytical X-ray Instruments Inc., Madison, WI, 1995. (b) Sheldrick, G. M. *SHELXS-97*, University of Göttingen, Göttingen, Germany, 1997. (c) Sheldrick, G. M. Crystal structure refinement with SHELXL. *Acta Crystallogr., Sect. A: Found. Crystallogr.* **2008**, *64*, 112−122. (d) *WinGX-Version 2014.1*, Farrugia, L. J. *J. Appl. Crystallogr.* **2012**, *45*, 849−854.10.1107/S0021889812029111
(13) Sheldrick, G. M. *SADABS Software for Empirical Absorption Correction*, University of Göttingen, Institute fur Anorganische Chemieder Universitat, Göttingen, Germany, 1999−2003.
(14) DIAMOND, Visual Crystal Structure Information System, version 3.1, Crystal Impact: Bonn, Germany, 2004.
(15) Liu, S.-Y.; Ma, Y. − P. Synthesis and crystal structures of dioxovanadium complexes with Schiff bases. *Synth. React. Inorg., Met.-Org., Nano-Met. Chem.* **2012**, *42* (4), 603−607.
(16) Deacon, G. B.; Phillips, R. J. Relationships between the carbon-oxygen stretching frequencies of carboxylato complexes and the type of carboxylate coordination. *Coord. Chem. Rev.* **1980**, *33*, 227−250.
(17) Pait, M.; Bauzá, A.; Frontera, A.; Colacio, E.; Ray, D. A new family of Ni_4 and Ni_6 aggregates from the self-assembly of $[Ni_2]$ building units: Role of carboxylate and carbonate bridges. *Inorg. Chem.* **2015**, *54* (10), 4709−4723.
(18) Nakamoto, K. *Infrared and Raman Spectra of Inorganic and Coordination Compounds*, 4th ed.; Wiley: New York, 1986.
(19) Kato, M.; Jonassen, H. B.; Fanning, J. C. Copper (II) complexes with subnormal magnetic moments. *Chem. Rev.* **1964**, *64*, 99−128.
(20) Buchanan, R. M.; Mashuta, M. S.; Oberhausen, K. J.; Richardson, J. F.; Li, Q.; Hendrickson, D. N. Active site model of urease: synthesis, structure, and magnetic properties of a binuclear nickel (II) complex containing a polyimidazole ligand. *J. Am. Chem. Soc.* **1989**, *111* (12), 4497−4498.
(21) Mandal, S.; Balamurugan, V.; Lloret, F.; Mukherjee, R. Syntheses, X-ray structures, and physicochemical properties of phenoxo-bridged dinuclear nickel (II) complexes: kinetics of trans-esterification of 2-hydroxypropyl-p-nitrophenylphosphate. *Inorg. Chem.* **2009**, *48* (16), 7544−7556.
(22) (a) Ghosh, A. K.; Bauza, A.; Bertolasi, V.; Frontera, A.; Ray, D. Dinuclear and heptanuclear nickel (II) complexes: Anion coordination induced ligand arm hydrolysis and aggregation around a nickel (II) core. *Polyhedron* **2013**, *53*, 32−39. (b) Chattopadhyay, T.; Mukherjee, M.; Mondal, A.; Maiti, P.; Banerjee, A.; Banu, K. S.; Bhattacharya, S.; Roy, B.; Chattopadhyay, D. J.; Mondal, T. K. A unique nickel system having versatile catalytic activity of biological significance. *Inorg. Chem.* **2010**, *49*, 3121−3129. (c) Biswas, A.; Das, L. K.; Drew, M. G. B.; Aromi, G.; Gamez, P.; Ghosh, A. Synthesis, crystal structures, magnetic properties and catecholase activity of double phenoxido-bridged penta-coordinated dinuclear nickel (II) complexes derived from reduced Schiff-base ligands: mechanistic inference of catecholase activity. *Inorg. Chem.* **2012**, *51*, 7993−8001.
(23) (a) Ghosh, A. K.; Shatruk, M.; Bertolasi, V.; Pramanik, K.; Ray, D. Self-Assembled Tetra-and Pentanuclear Nickel (II) Aggregates From Phenoxido-Based Ligand-Bound {Ni2} Fragments: Carboxylate Bridge Controlled Structures. *Inorg. Chem.* **2013**, *52*, 13894−13903. (b) Pait, M.; Bauzá, A.; Frontera, A.; Colacio, E.; Ray, D. A New Family of Ni_4 and Ni_6 Aggregates from the Self-Assembly of $[Ni_2]$ Building Units: Role of Carboxylate and Carbonate Bridges. *Inorg. Chem.* **2015**, *54*, 4709−4723. (c) Jana, M. S.; Priego, J. L.; Jiménez-Aparicio, R.; Mondal, T. K. Novel tetranuclear Ni (II) Schiff base complex containing Ni_4O_4 cubane core: Synthesis, X-ray structure, spectra and magnetic properties. *Spectrochim. Acta, Part A* **2014**, *133*, 714−719. (d) Mandal, D.; Bertolasi, V.; Ribas-Ariño, J.; Aromí, G.; Ray, D. Self-Assembly of an Azido-Bridged $[Ni^{II}_6]$ Cluster Featuring Four Fused Defective Cubanes. *Inorg. Chem.* **2008**, *47*, 3465−3467.
(24) Chilton, N. F.; Anderson, R. P.; Turner, L. D.; Soncini, A.; Murray, K. S. PHI: A powerful new program for the analysis of anisotropic monomeric and exchange-coupled polynuclear d-and f-block complexes. *J. Comput. Chem.* **2013**, *34*, 1164−1175.
(25) (a) Karmakar, S.; Khanra, S. Polynuclear coordination compounds: a magnetostructural study of ferromagnetically coupled Ni_4O_4 cubane core motif. *CrystEngComm* **2014**, *16*, 2371−2383. (b) Clemente-juan, J. M.; Chansou, B.; Donnadieu, B.; Tuchagues, J. P. Synthesis, structure, and magnetic properties of the low-symmetry tetranuclear cubane-like nickel complex $[Ni_4(pypentO)\ (pym)(\mu_3\text{-}OH)_2(\mu\text{-}Oac)_2(NCS)_2(OH_2)]$. *Inorg. Chem.* **2000**, *39*, 5515−5519. (c) Halcrow, M. A.; Sun, J. S.; Huffman, J. C.; Christou, G. Structural and magnetic properties of $[Ni_4(\mu_3\text{−}OMe)_4(dbm)_4(MeOH)_4]$ and $[Ni_4(\eta_1,\mu_3\text{−}N_3)_4(dbm)_4(EtOH)_4]$. Magnetostructural correlations for $[Ni_4X_4]^{4+}$ cubane complexes. *Inorg. Chem.* **1995**, *34*, 4167−4177.
(26) Das, A.; Klinke, F. J.; Demeshko, S.; Meyer, S.; Dechert, S.; Meyer, F. Reversible solvatomagnetic effect in novel tetranuclear cubane-type Ni_4 complexes and magnetostructural correlations for the $[Ni_4(\mu_3\text{-}O)_4]$ core. *Inorg. Chem.* **2012**, *51*, 8141−8149.
(27) (a) Alexopoulou, K. I.; Raptopoulou, C. P.; Psycharis, V.; Terzis, A.; Tangoulis, V.; Stamatatos, T. C.; Perlepes, S. P. Solvent-dependent access to two different Ni^{II}_4 core topologies from the first use of pyridine-2,6-dimethanol in nickel (II) cluster chemistry. *Aust. J. Chem.* **2012**, *65*, 1608−1619. (b) Iijima, F.; Hasumi, K.; Shiga, T.; Newton, G. N.; Oshio, H. Linking magnetic clusters: Ferrimagnetic interactions in a nonanuclear nickel(II) cluster. *Chem. Lett.* **2012**, *41*, 691−692. (c) Efthymiou, C. G.; Papatriantafyllopoulou, C.; Alexopoulou, N. I.; Raptopoulou, C. P.; Boča, R.; Mrozinski, J.; Bakalbassis, E. G.; Perlepes, S. P. A mononuclear complex and a cubane cluster from the initial use of 2-(hydroxymethyl) pyridine in nickel (II) carboxylate chemistry. *Polyhedron* **2009**, *28* (15), 3373−3381. (d) Aromí, G.; Batsanov, A. S.; Christian, P.; Helliwell, M.; Roubeau, O.; Timco, G. A.; Winpenny, R. E. Synthesis, structure and magnetic properties of hydroxyquinaldine-bridged cobalt and nickel cubanes. *Dalton Trans.* **2003**, 4466−4471.
(28) (a) Cortijo, M.; Delgado-Martinez, P.; González-Prieto, R.; Herrero, S.; Jiménez-Aparicio, R.; Perles, J.; Priego, J. L.; Torres, M. R. Microwave and solvothermal methods for the synthesis of nickel and ruthenium complexes with 9-anthracene carboxylate ligand. *Inorg. Chim. Acta* **2015**, *424*, 176−185. (b) Piovezan, C.; Silva, J. M. R.; Neves, A.; Bortoluzzi, A. J.; Haase, W.; Tomkowicz, Z.; Castellano, E. E.; Hough, T. C.; Rossi, L. M. Design of a dinuclear nickel (II) bioinspired hydrolase to bind covalently to silica surfaces: synthesis, magnetism, and reactivity studies. *Inorg. Chem.* **2012**, *51*, 6104−6115. (c) Greatti, A.; Scarpellini, M.; Peralta, R. A.; Casellato, A.; Bortoluzzi, A. J.; Xavier, F. R.; Jovito, R.; de Brito, M. A.; Szpoganicz, B.; Tomkowicz, Z.; Rams, M. Synthesis, structure, and physicochemical properties of dinuclear Ni^{II} complexes as highly efficient functional models of phosphohydrolases. *Inorg. Chem.* **2008**, *47*, 1107−1119. (d) Sakiyama, H.; Suzuki, T.; Ono, K.; Ito, R.; Watanabe, Y.; Yamasaki, M.; Mikuriya, M. Synthesis, structure, and magnetic properties of dinuclear nickel(II) complexes with a phenol-based dinucleating ligand with four methoxyethyl chelating arms. *Inorg. Chim. Acta* **2005**, *358* (6), 1897−1903. (e) Adams, H.; Bradshaw, D.; Fenton, D. E. Dinuclear nickel(II) and zinc(II) complexes of 2,6-bis[{bis(2-pyridylmethyl)amino}methyl]-4-methylphenol. *Inorg. Chim. Acta* **2002**, *332* (1), 195−200.

DOI: 10.1021/acs.inorgchem.6b02015
Inorg. Chem. 2016, 55, 10783−10792